Electronic Supplementary Information

Real-time visual determination of the flux of hydrogen sulphide using a hollow-channel paper electrode

Li Li,[a] Yan Zhang,[a] Fang Liu,[a] Min Su,[a] Linlin Liang,[a] Shenguang Ge[b] and Jinghua Yu*[a]

[a] School of Chemistry and Chemical Engineering, University of Jinan, Jinan 250022, P.R. China.

[b]Shandong Provincial Key Laboratory of Preparation and Measurement of Building Materials, School of Material Science and Engineering, University of Jinan, Jinan 250022, P.R. China.

* Corresponding to: E-mail address: ujn.yujh@gmail.com
Tel: +86-531-82767161
Fax: +86-531-82765956

Materials and methods

Reagents

All chemicals and solvents used here were aseptic after heat sterilization treatment. Chloroplatinic acid (H_2PtCl_6) was obtained from Shanghai Chemical Reagent Company (Shanghai, China). Ascorbic acid (AA, ≥99.0%), N-hydroxysuccinimide (NHS), 1-ethyl-3-(3-dimethylaminopropyl) carbodiimide (EDC) and vascular endothelial growth factor (VEGF) were purchased from Sigma. All chemicals and solvents were used as received with the analytical grade or above. Ultrapure water obtained from a Millipore water purification system (>18.2 MΩ.cm, Milli-Q, Millipore) was used in all assays and solutions.

The human breast cancer cells MCF-7 and HeLa cells were provided by Shandong Tumor Hospital. The aptamer used in this study was purchased from Sangon Biotech Co., Ltd. (Shanghai, China), and the sequences of oligonucleotides were listed as follows:

Aptamer for MCF-7 cell: 5′-GCAGTTGATCCTTTGGATACCCTGGTTTTT TTT TTT-NH_2-3′.

Aptamer for HeLa cell: 5′-TTGGTGGTGGTGGTTGTG GTGGTGGTGG-NH_2 -3′

0.1 M phosphate buffer solution (PBS, pH 7.4) containing 0.05 M $S_2O_8^{2-}$, 1 μM Cu^{2+} was employed as the supporting electrolyte in ECL analysis. Carbon ink (ED423ss) and Ag/AgCl ink (CNC-01) were purchased from Acheson. Whatman chromatography paper #1 (58.0 cm × 68.0 cm) (pure cellulose paper) was obtained from GE Healthcare Worldwide (Pudong Shanghai, China) and used with further adjustment of size (A4 size).

Apparatus

Ultraviolet-visible (UV-vis) absorption spectra were recorded on a UV-2550 spectrophotometer (Shimadzu, Japan). Scanning electron microscopy (SEM) images were obtained using a QUANTA FEG 250 thermal field emission scanning electron microscope (FEI Co., USA). X-ray photoelectron spectra (XPS) were measured using an ESCALAB 250 spectrometer (Thermo Fisher Scientific) with monochromatized Al-Kα X-ray radiation (1486.6 eV) in ultrahigh vacuum ($<10^{-7}$ Pa). Transmission electron microscopy (TEM) images were obtained from a JEOL JEM-1400

microscope (Japan). Electrochemical impedance spectroscopy (EIS) was performed on an IM6x electrochemical station (Zahner, Germany).

Preparation of GQDs

The preparation of bGQDs was similar to a previous protocol [1] with slight modifications and the procedure was described below. 2 g Citric acid was put into a 5 mL beaker and heated to 200 °C using a heating mantle. About 5 min later, the CA was liquated. Subsequently, the color of the liquid was changed from colorless to pale yellow, and then orange in 30 min, implying the formation of bGQDs.

Fabrication of Au@Pt-PWE

The Au@Pt-PWE with enhanced conductivity and enlarged surface area was fabricated through seed-mediated synthetic method and detailed procedure were described as follows: Firstly, as-prepared Au NPs seeds solution (15 μL) [2] was added to one working zone. Then the origami device was equilibrated for 2 h. After rinsing with water thoroughly according to the method in our previous work [3] to remove loosely bound Au NPs seeds, freshly prepared growth aqueous solution (15 μL) of PBS (pH 7.4) containing AA (100 mM), $HAuCl_4$ (10 mM) and H_2PtCl_6 (10 mM) was applied into the Au NPs seeded PWE, and incubated for 10 min. Then, the resulting Au@Pt-PWE was washed with Milli-Q water thoroughly, and dried at room temperature for 30 min.

Cell culture

MCF-7 (human breast carcinoma) and HeLa cells were cultured in dulbecco's modified eagle medium (DMEM) supplemented with 10% fetal bovine serum and 1% penicillin/streptomycin. Cultures were maintained at 37 °C and in 5% CO_2 atmosphere. The culture medium was changed every other day and the cells were passaged when they reached 80-90% confluency. For tumor cell ECL measurement, cells were placed inside a 12-well plate. When cultured for two days, tumor cells were digested by pancreatic enzymes and dispersed in PBS. After being blown well, tumor cells were counted by a Petroff-Hausser cell counter (U.S.A.). Cell number was determined using a Petroff-Hausser cell counter (U.S.A.).

Fabrication and characterization of this 3D origami ECL device

The 3D paper-based ECL device was fabricated using a previously reported method [4] and a detailed procedure was described below. A wax-printing technique was used to create the 3D paper-based ECL device because this fabrication process is

simpler, less expensive, and faster than other reported methods [5,6]. Wax was used as the paper hydrophobization and insulation agent in this work to construct hydrophobic barrier on paper. The shape of hydrophobic barrier on origami device was designed using Adobe illustrator CS4 and the entire origami device could be produced in bulk on an A4 paper sheet by a commercially available solid-wax printer (FUJIXEROX Phaser 8560DN, Japan) (Scheme S1A,B and Fig. S1). This origami device was comprised of a hollow channels (30.0 mm × 30.0 mm), one square sample tabs and auxiliary tab (30.0 mm × 30.0 mm). There were four circular zones on the sample/auxiliary tab for screen-printing working/reference and counter electrodes, respectively (Scheme S1C). The white color in Scheme S1C indicates the position of the HC. The green and yellow wax colors were used to form the barriers and the floor of the HC, respectively. Owing to the porous structure of paper, the melted wax can penetrate into the paper network to decrease the hydrophilicity of paper remarkably (Fig. S2 and Fig. S3). After the paper was placed in an oven at 150 °C for 120 s, the unprinted area still maintained good hydrophilicity, flexibility, and porous structure and will not affect the further screen-printing of electrodes and modifications. Then, the wax-penetrated paper sheet was ready for screen-printing of electrode. The electrode array consisted of four screen-printed carbon working electrodes (5 mm in diameter) on the sample tab and four screen-printed carbon counter electrodes and four Ag/AgCl reference electrodes (7 mm in diameter) on the auxiliary tab (Scheme S1C and Fig. S4), respectively (every two working electrodes for one tumor cells). Via hole on the sample tab was covered by an AuNPs layer to make both side of the sample tab conductive, which was sealed by silver on the reverse side of sample tab (Fig. S5). Finally, the paper sheet was cut into individual origami paper-based analytical device for further modifications. After folding at the predefined fold line (1 mm in width), the three screen-printed electrodes would be connected once the paper ECL cell was filled with solution.

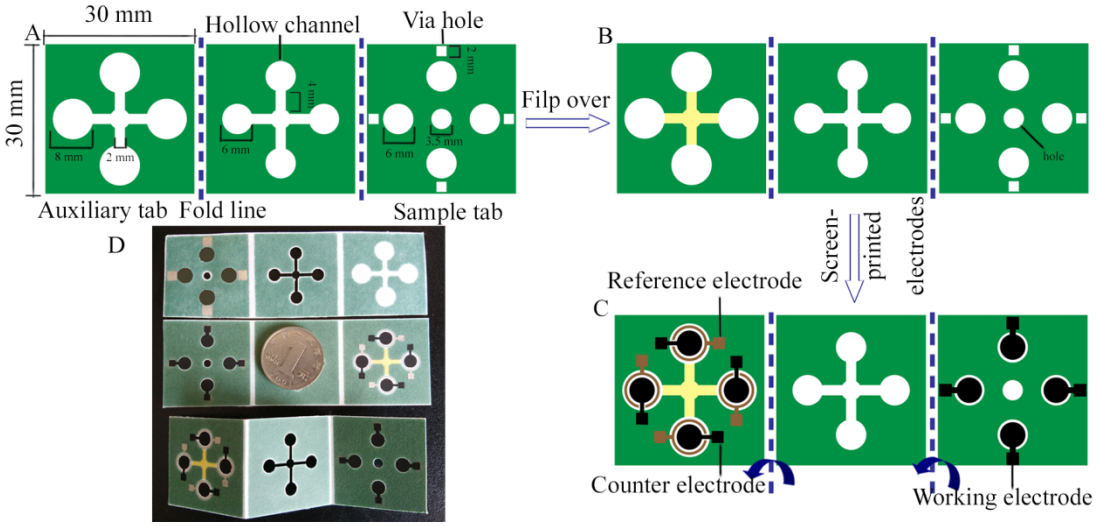

Scheme S1 The schematic representation, size, and shape of this 3D paper-based ECL device. Paper sheets were firstly patterned in bulk using a wax printer. Then electrodes were screen-printed on A4 paper sheet in bulk. After laser cut and modification, the device was used to detect H_2S released from tumor cells.

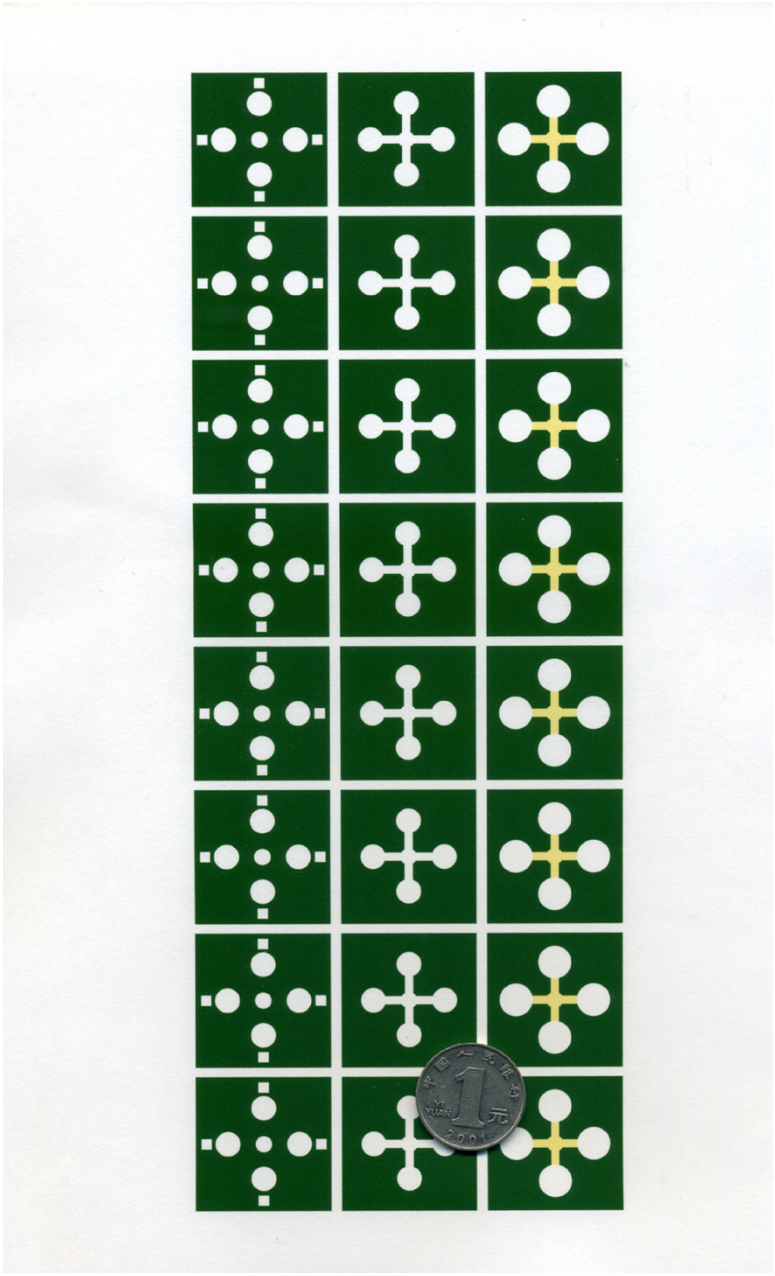

Fig. S1. Wax-patterns of this HC-PEOC on a paper sheet (A4) before baking.

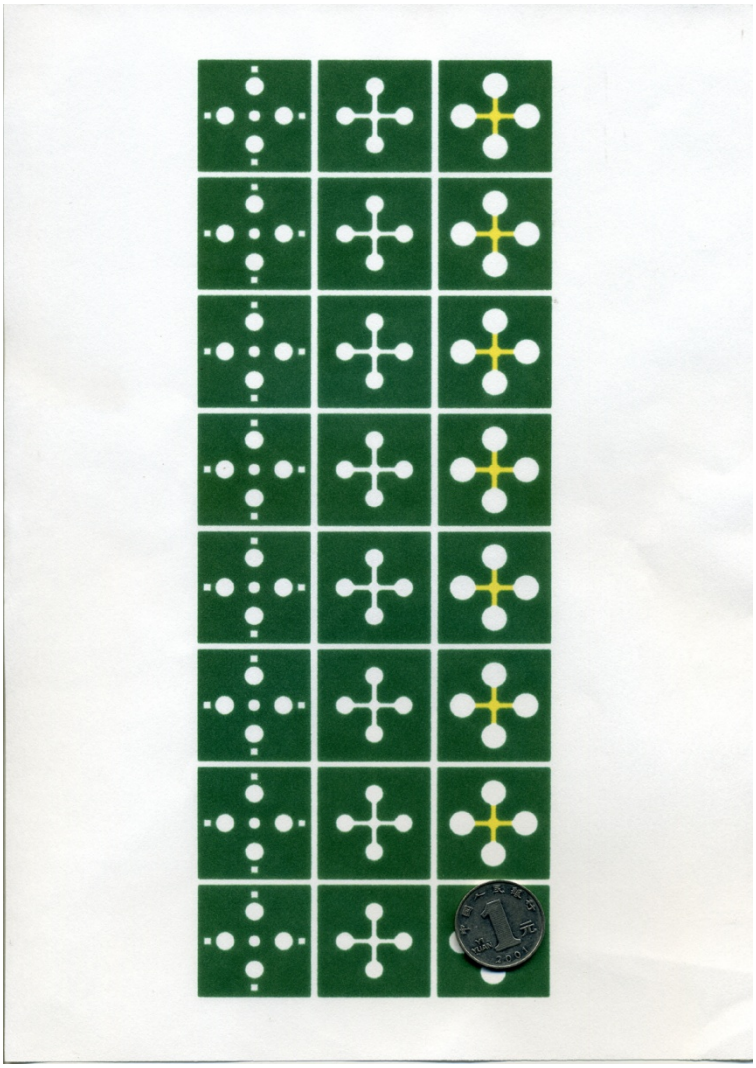

Fig. S2. Wax-patterns of this HC-PEOC on a paper sheet (A4) after baking.

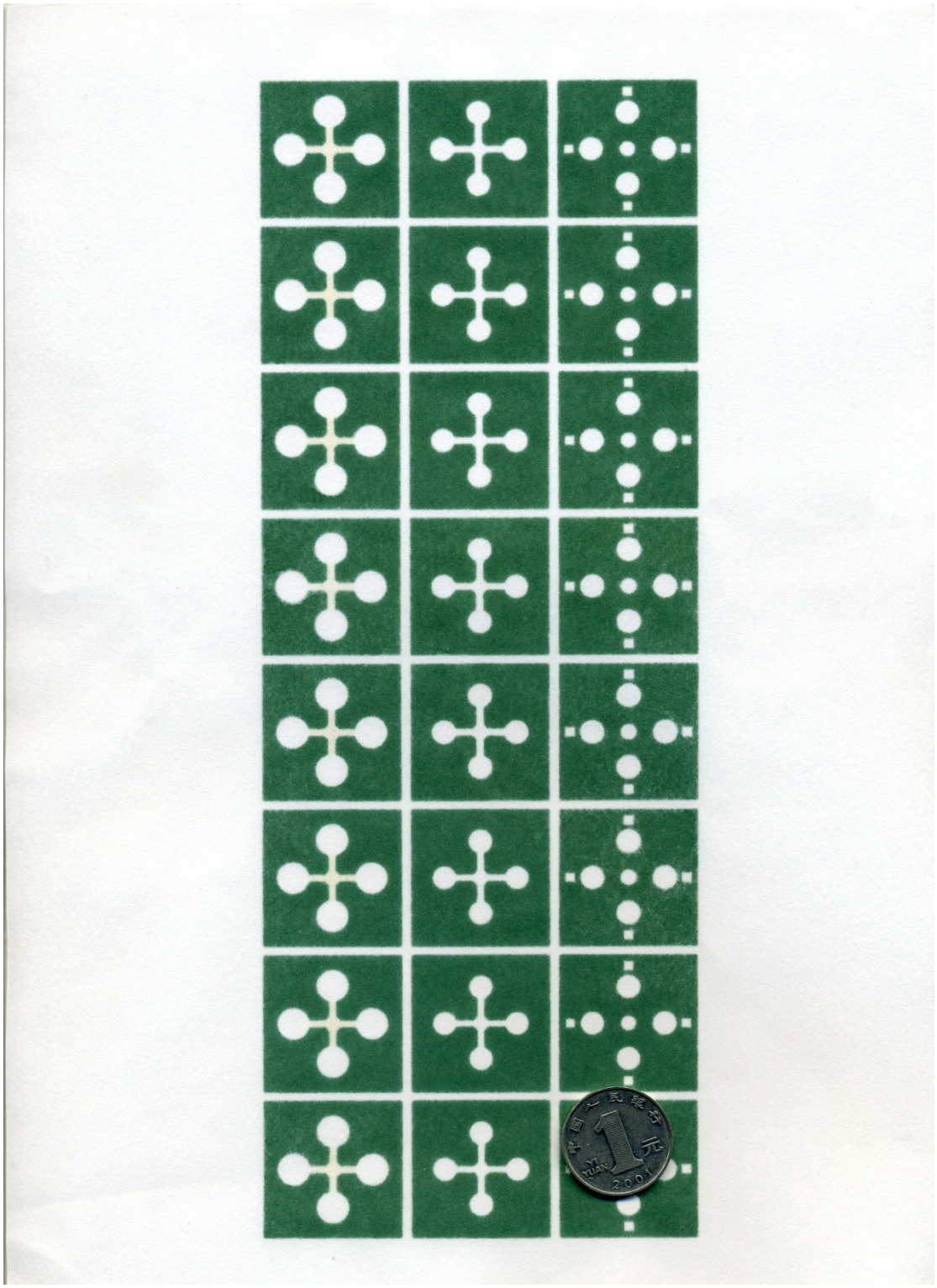

Fig. S3. Reverse side of wax-patterns of this HC-PEOC on a paper sheet (A4) after baking.

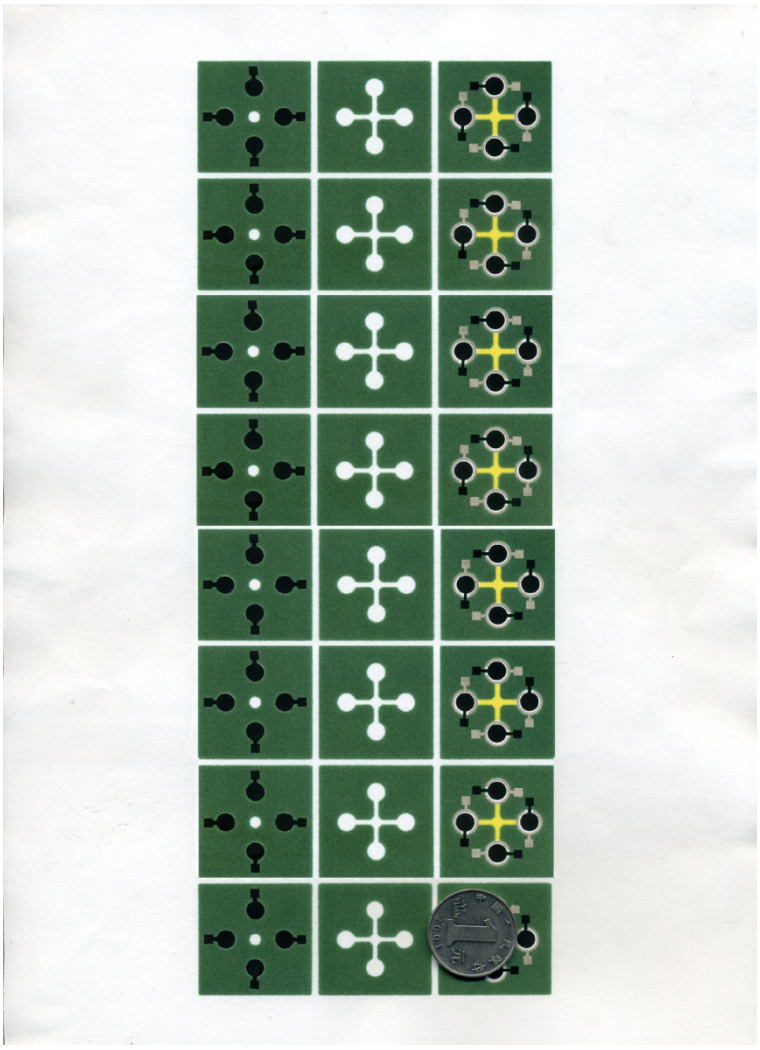

Fig. S4. HC-PEOC on a paper sheet (A4) after screen-printing electrodes.

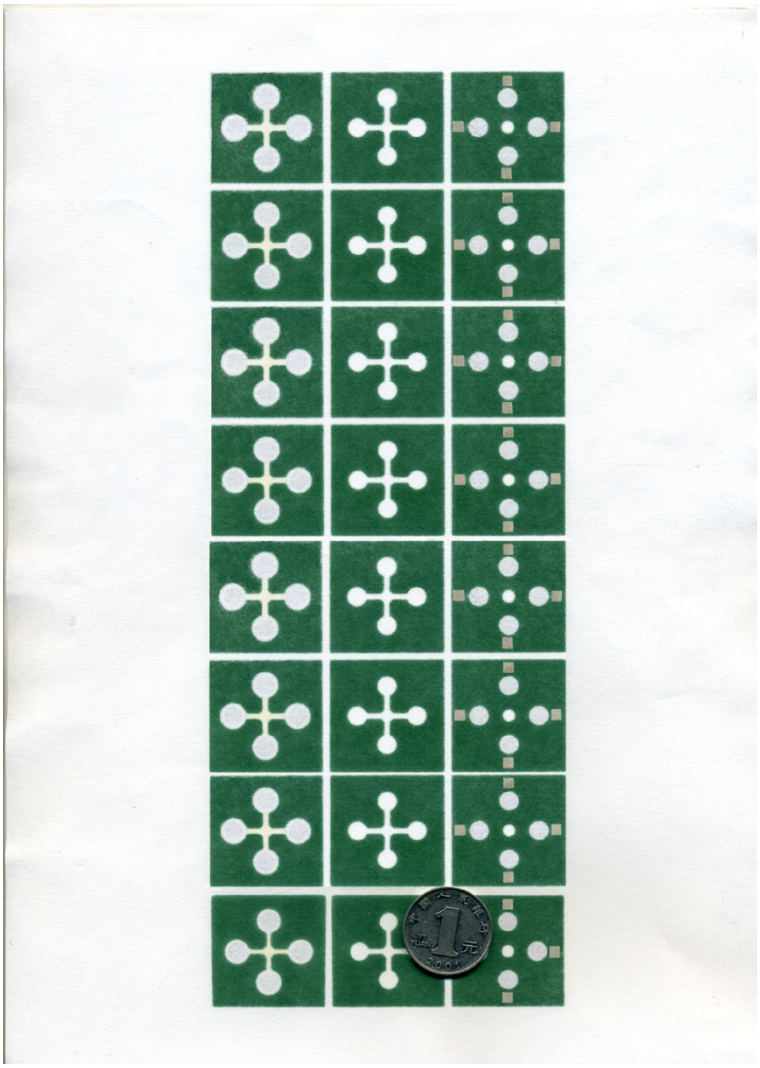

Fig. S5. Reverse side of HC-PEOC on a paper sheet (A4) after screen-printing electrodes.

Electrical resistivity of Au@Pt core-shell nanoparticles grown paper sample zone

To measure the resistivity of Au@Pt core-shell NPs grown paper sample zone, Au@Pt core-shell NPs modified rectangular wax-penetrated paper zones (1.0 mm×20.0 mm) with screen-printed carbon ink on one side were fabricated through the growth of an interconnected Au@Pt layer on the surfaces of cellulose fibers in these rectangular paper zones under the same conditions in each case, the average resistivity of which equaled to the resistivity of Au@Pt modified paper sample zone of Au@Pt-PWE in this work. Prior to the measurements, both the bare and Au@Pt core-shell NPs grown rectangular paper zones were dried in a drying oven for 3 h. Then the measurement was performed using a DT-830 multimeter (UniVolt, Japan).

Characterizations of bGQDs

To characterize the structure and morphology of the as-prepared bGQDs, TEM

observations were conducted. As shown in Fig. S6A, TEM image suggested that the size of the bGQDs had a uniform shape and was narrowly distributed with diameters in the range of 5~6 nm.

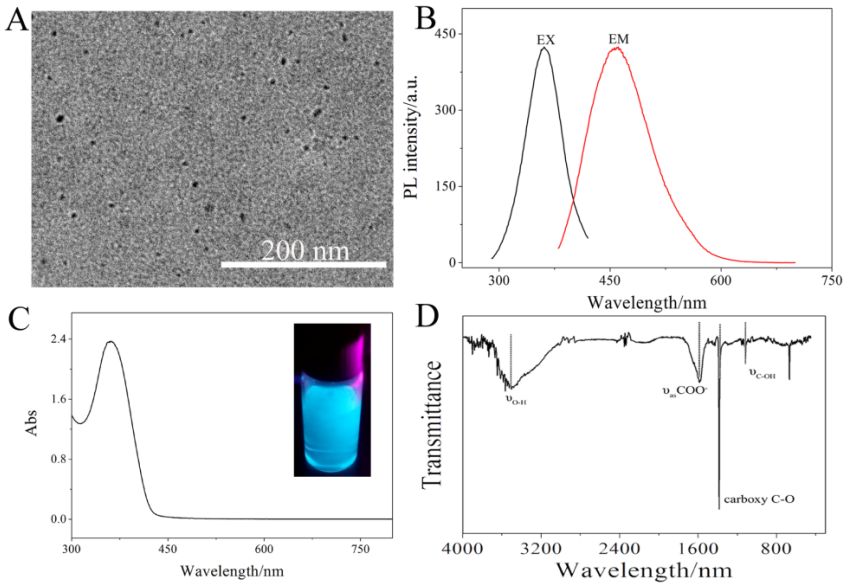

Fig. S6. (A) TEM and (B) FL of the obtained bGQDs; (C) UV-vis spectrum of the obtained bGQDs. Inset: photograph of bGQDs taken under UV light. (D) FTIR spectra of the prepared bGQDs.

To further explore the optical properties of the bGQDs, PL spectra was studied (Fig. S6B). First of all, the emission wavelength of bGQDs is nearly excitation-independent (Fig. S7), with the maximum excitation wavelength and the maximum emission wavelength at 362 and 460 nm, respectively. The excitation-independent emission of the bGQDs implies that both the size and the

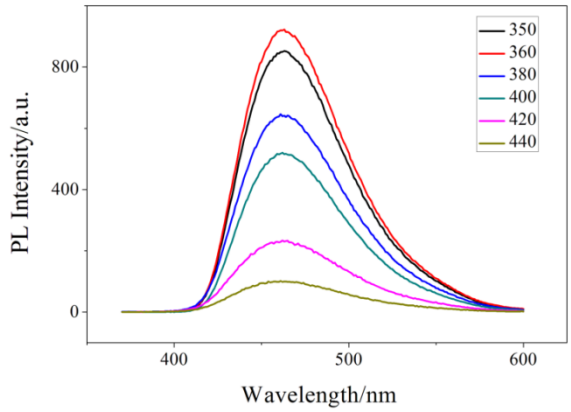

Fig. S7. Emission spectra of the bGQDs with excitation of different wavelength.

surface state of those sp^2 clusters contained in bGQDs should be uniform. For the UV-vis absorption of bGQDs (Fig. S6C), a well-defined absorption band at 365 nm can be observed and the wavelength of the absorption peak of bGQDs in UV-vis absorption spectra was almost the same as that of the excitation peak of bGQDs. The GQDs aqueous solutions exhibited blue fluorescence excited by 365 nm lamp (inset). FTIR was used to characterize the obtained bGQDs (Fig. S6D). In the FTIR spectra, the bGQDs showed C-OH group (alkoxy) stretching peak at 1113 cm^{-1} and C–O (carboxy) deformation peak at 1389 cm^{-1} and O-H group (carboxy) stretching peak at 3458 cm^{-1}, showing that the obtained bGQDs contain –COOH and –OH groups.

Characterization of this HC-PEOC

EIS was used to verify the assembly processes of the modified electrodes step by step. The impedance spectra are shown in Fig. S8. The Nyquist plot comprises a semicircular part at higher frequency range and a straight linear part at lower frequency range. The diameter of the semicircle equals the electron transfer resistance (R_{et}) at the electrode interface. Due to the good electronic transfer ability, the Au@Pt-modified PWE (curve b) exhibited lower R_{et} than bare PWE (curve a).

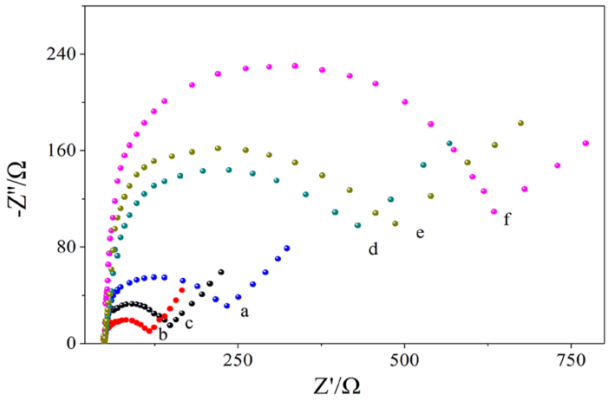

Fig. S8. EIS of the PWE under different conditions: a) bare PWE, b) Au@Pt-PWE, c) GQDs/Au@Pt-PWE, d) aptamer/GQDs/Au@Pt-PWE, e) BSA/aptamer/GQDs/Au@Pt-PWE, (f) MCF-7/BSA/aptamer/GQDs/Au@Pt-PWE were carried out in 10 mM $[Fe(CN)_6]^{3-/4-}$ containing 0.5 M KCl.

After the bGQDs were assembled on Au@Pt-modified PWE, the R_{et} increased slightly (curve c), which was attributed to the electronegative carboxyl groups of bGQDs repelling the transfer of the negatively charged probe $[Fe(CN)_6^{3-/4-}]$. Subsequently, the diameter of the semicircles increased successively with sequential assembly of aptamers (curve d), BSA (curve e) and cells (curve f), showing the step-by-step increase of R_{et}, which indicates the successful assembly of the biosensor.

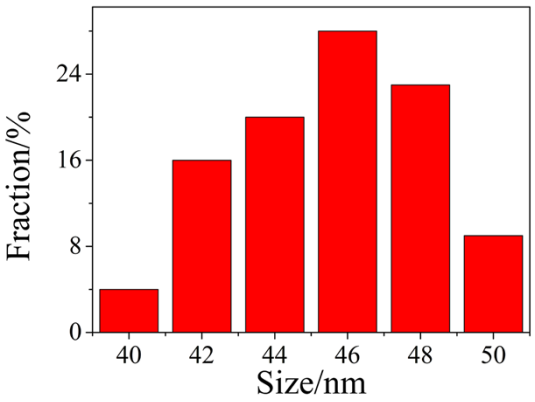

Fig. S9. Size distributions of Au@Pt NPs.

Detection of H_2S standard solution at our tumor cell immobilized Au@Pt-PWE

Our work aimed at developing a biosensor for monitoring the release process and measuring the flux of H_2S from cells. To demonstrate the sensitivity of our H_2S detection method, Au@Pt-PWE was treated with H_2S under a series of different concentrations to obtain a standard curve of ECL intensity versus H_2S concentration.

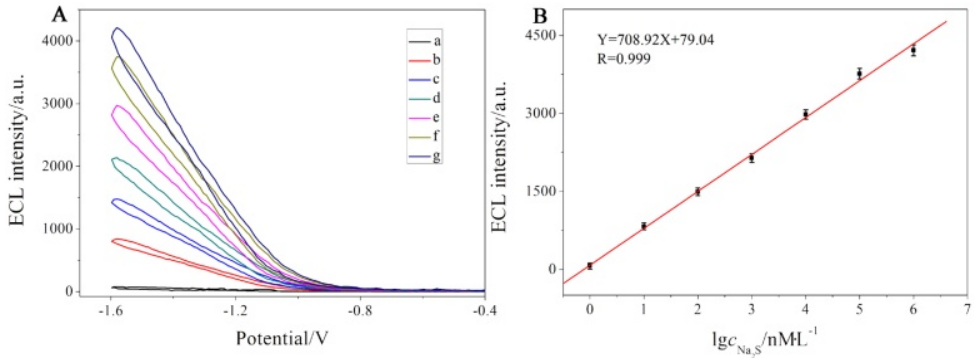

Fig. S10. The ECL responses of the tumor cells immobilized Au@Pt-PWE towards various concentrations of Na_2S in 20 μL PBS (pH 7.4) containing 0.05 M $S_2O_8^{2-}$, 1 μM Cu^{2+} (A); calibration curve for Na_2S determination (B).

And the potential swept sweeping range from 0 to -1.6 V with a scan rate of 100 mV s^{-1} after 20 μL of PBS buffer solution (pH 7.4) was added. PBS buffer containing 0.05 M $S_2O_8^{2-}$, 1 μM Cu^{2+} and different concentrations of Na_2S (a common hydrogen sulphide donor) standard solution were used in this experiment as detection solution. The typical response curve (Fig. S10) shows that the ECL response was directly proportional to the concentration logarithm in the range 1.0 nM-1.0 mM for H_2S and the detection limit was 0.35 nM (S/N=3).

Optimization of experiment conditions

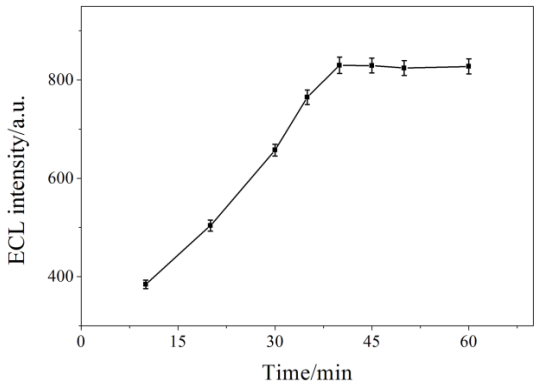

Fig. S11. Effect of incubation time for the specific recognition of the aptamer and MCF-7 cells.

The incubation time for cells in the BSA/aptamer/GQDs/Au@Pt-PWE is an important parameter for the specific recognition of the aptamer and cells. After incubating with MCF-7 cells suspension for 40 min, it can be seen that the ECL value reached a steady value even if a longer time was applied, indicating tendency of thorough capture of MCF-7 cells in the BSA/aptamer/GQDs/Au@Pt-PWE (Fig. S11). Thus, the optimal conditions of the cytosensor were 40 min for cell capture.

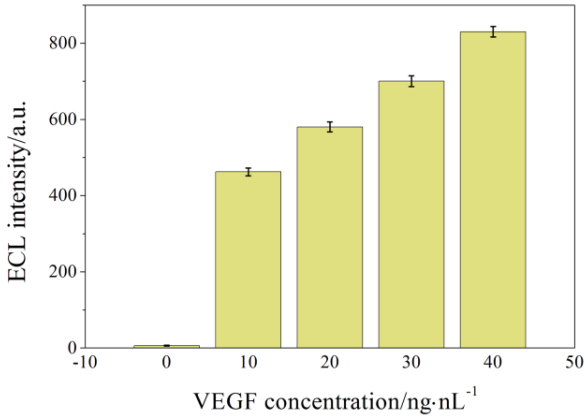

Fig. S12. Dependence of the flux of H_2S released from the cells on the concentration of VEGF.

In addition, the effect of VEGF dose on the HC-PEOC sensor signals was evaluated using the developed method. As shown in Fig. S12, an increase of ECL intensity was observed with the VEGF concentration range from 10-40 $ng \cdot nL^{-1}$, which indicates the flux of H_2S release from the MCF-7 cells significantly increases with enhancement of the VEGF dose, showing a VEGF dose-dependent trend.

Specificity, reproducibility, and stability of the HC-PEOC

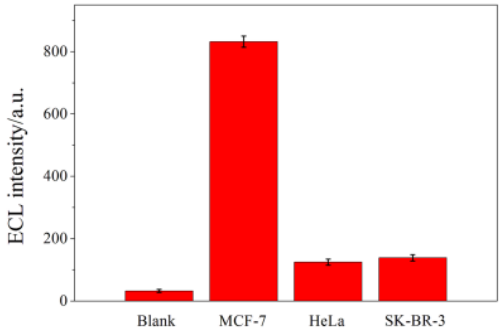

Fig. S13. ECL response of the HC-PEOC with different cell lines at a concentration of 1.0×10^4 cells mL^{-1}.

The specific recognition between aptamer and target cells was evaluated by incubating three different cells in BSA/aptamer/GQDs/Au@Pt-PWE. As shown in Fig. S13, a significant increase in the ECL intensity from MCF-7 cells/aptamer/GQDs/Au@Pt-PWE was observed. However, only slightly increase of the ECL response was observed in the other cells/aptamer/GQDs/Au@Pt-PWEs, suggesting the acceptable specificity of the cytosensor for MCF-7 cells. Meanwhile, the biosensor showed the relative standard deviation of 4.6% examined for four determinations at the cell concentrations of 1.0×10^4 cells·mL^{-1}, which shows the good reproducibility of the biosensor. To investigate the stability of this HC-PEOC, it was stored in a sterile valve bag at 4 °C and measured at intervals of three days, no obvious change was observed after three weeks. Thus, the as-proposed cytosensor exhibited good performance in detection of H_2S released from cancer cells with broad detection range, low detection limit, and good stability and reproducibility.

Detection of H_2S released from HeLa cells using HC-PEOC

We quantitatively assayed cellular H_2S based on the H_2S concentration-dependent ECL responds. As shown in Fig. S14, with the increasing concentrations of HeLa cells, good correlations between the ECL peak intensity and the logarithm of the HeLa cells concentration in the range from 1.0×10^3 cells·mL^{-1} to 5.0×10^6 cells·mL^{-1} (Fig. S14B) was observed. The ECL intensity of 1936 a.u. was obtained after incubation of 1.0×10^5 cells·mL^{-1} (10 μL), corresponding to $(4.13\pm0.2) \times10^{-7}$ M of H_2S being released from each cell which was estimated based on the calibration curve depicted in the Fig. S10 and the number of cells used in the measurements (~1.0×10^5 cells·mL^{-1}).

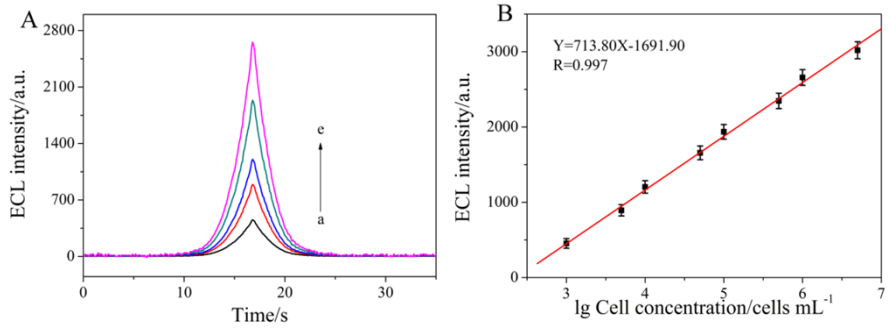

Fig. S14. A) Typical ECL responses of this HC-PEOC incubated with different concentrations of HeLa cells (from a to e: 10^3, 5×10^3, 10^4, 10^5, and 10^6 cells mL^{-1}, respectively); B) Relationship between ECL response and cell concentration.

References

[1] Y.Q. Dong, J.W. Shao, C.Q. Chen, H. Li, R.R. Wang, Y.W. Chi, X.M. Lin, G.N. Chen, *Carbon,* 2012, **50**, 4738.

[2] L.B. Wang, Y.Y. Zhu, L.G. Xu, W. Chen, H. Kuang, L.Q. Liu, A. Agarwal, C.L. Xu, N.A. Kotov, *Angew. Chem. Int. Ed.,* 2010, **49**, 5472.

[3] J.X. Yan, L. Ge, X.R. Song, M. Yan, S.G. Ge, J.H. Yu, *Chem. Eur. J.*, 2012, **18**, 4938.

[4] L.N. Zhang, Y.H. Wang, C. Ma, P.P. Wang, M. Yan, *RSC Adv.,* 2015, **5**, 24479.

[5] Y. Lu, W.W. Shi, L. Jiang, J.H. Qin, B.C. Lin, *Electrophoresis,* 2009, **30**, 1497.

[6] E. Carrilho, A.W. Martinez, G.M. Whitesides, *Anal. Chem.,* 2009, **81**, 7091.